Transition from suppressed to active convection modulated by a weak-temperature gradient derived large-scale circulation

Transition from Suppressed to Active Convection Modulated by a Weak Temperature Gradient–Derived Large-Scale Circulation

C. L. DALEU, S. J. WOOLNOUGH, AND R. S. PLANT

Department of Meteorology, University of Reading, Reading, United Kingdom

(Manuscript received 19 February 2014, in final form 24 July 2014)

ABSTRACT

Numerical simulations are performed to assess the influence of the large-scale circulation on the transition from suppressed to active convection. As a model tool, the authors used a coupled-column model. It consists of two cloud-resolving models that are fully coupled via a large-scale circulation that is derived from the requirement that the instantaneous domain-mean potential temperature profiles of the two columns remain close to each other. This is known as the weak temperature gradient approach.

The simulations of the transition are initialized from coupled-column simulations over nonuniform surface forcing, and the transition is forced in the dry column by changing the local and/or remote surface forcings to uniform surface forcing across the columns. As the strength of the circulation is reduced to zero, moisture is recharged into the dry column and a transition to active convection occurs once the column is sufficiently moistened to sustain deep convection. Direct effects of changing surface forcing occur over the first few days only. Afterward, it is the evolution of the large-scale circulation that systematically modulates the transition. Its contributions are approximately equally divided between the heating and moistening effects.

A transition time is defined to summarize the evolution from suppressed to active convection. It is the time when the rain rate in the dry column is halfway to the mean value obtained at equilibrium over uniform surface forcing. The transition time is around twice as long for a transition that is forced remotely compared to a transition that is forced locally. Simulations in which both local and remote surface forcings are changed produce intermediate transition times.

1. Introduction

Convection and cloud-related processes are the dominant features of the weather of the tropics. The associated heat release is an essential source of energy for the large-scale tropical dynamics, and the large-scale dynamics in turn often acts as a forcing mechanism for convection. The interactions between tropical deep convection and large-scale tropical dynamics regulate the tropical climate, so a good representation of these interactions in the numerical models used for weather forecast and climate prediction is essential. General circulation models (GCMs) aim to provide a good representation of the large-scale flow, but because of the large difference of scales between individual convective clouds and the large-scale circulation, the effects of the clouds themselves on the large-scale circulation must be represented through a convective parameterization scheme (e.g., Tiedtke 1989; Gregory and Rowntree 1990; Kain 2004). On the other hand, cloud-resolving models (CRMs) aim to provide a good representation of convective clouds, but, as used in the traditional way, the large-scale circulation is prescribed (e.g., Grabowski et al. 2006; Woolnough et al. 2010; Fridlind et al. 2012).

To understand how convection influences the evolution of the large-scale flows and how the large-scale flows in turn influence the evolution of convection, there is a need for approaches in which the large-scale flows and convection are both simulated. CRMs run over a domain on the order of the large-scale circulation (≈10 000 km) or GCMs run with very high horizontal resolution are currently the most realistic models that

Denotes Open Access content.

Corresponding author address: C. L. Daleu, Department of Meteorology, University of Reading, Earley Gate, P.O. Box 243, Reading RG6 6BB, United Kingdom.
E-mail: c.daleu@reading.ac.uk

DOI: 10.1175/JAS-D-14-0041.1

explicitly simulate both moist convection and large-scale tropical circulations and, hence, the interactions between them. Typically, such models are very expensive to run, so that they are not practical for sensitivity experiments. As a result, in normal practice the domain for CRMs is usually limited to a size that does not allow for the representation of the large-scale flows while the grid spacing for GCMs is usually increased to a size that does not allow for explicit simulation of convection. Studies that have explicitly simulated moist convection and the large scale include experiments conducted at the Earth Simulator Center (e.g., Liu et al. 2009) and in projects such as Cascade (e.g., Holloway et al. 2012). An alternative simulation approach is superparameterization (e.g., Randall et al. 2003), in which a CRM is embedded into each grid square of a GCM. A further alternative is to reduce artificially the scale difference between convection and large-scale flow such that both can be simulated with relative ease (Kuang et al. 2005; Bechtold et al. 2013).

To study the interactions between convection and the large scale at a reasonable computational cost, one possible method is to parameterize the large-scale circulation to which a limited-area model is subject and to allow interactions of this circulation with the simulated convection. Many studies that have followed this method parameterize a suitable large-scale circulation for the tropical atmosphere by relying on the physical principle that gravity waves over a large area of the tropics are very effective at redistributing density anomalies produced by surface fluxes or radiation such that near-uniform density is maintained on isobaric surfaces (Bretherton and Smolarkiewcz 1989; Mapes and Houze 1995; Yano and Bonazzola 2009). This physical principle is valid only near the equator where the action of the Coriolis force is almost zero. In such an area, horizontal gradients and time tendencies of potential temperature are both negligible compared to its vertical gradients. A large-scale vertical velocity can then be derived as that which is sufficient to offset the simulated convective heating and accordingly maintain the horizontal domain-mean potential temperature.

An example of a study of this nature is that of Sobel and Bretherton (2000), in which the authors derived a large-scale circulation that completely consumes the sources of potential temperature and thus maintains the horizontal gradients of potential temperature at zero at all times. From their study, the use of this approach has become known as the weak temperature gradient (WTG) approximation. Most subsequent WTG studies have imposed a weaker constraint that the parameterized large-scale circulation consumes the source of potential temperature over some nonzero but short time scale (e.g., Raymond and Zeng 2005; Sobel et al. 2007; Sessions et al. 2010; Daleu et al. 2012; this study).

The WTG approximation has proved to be a useful and computationally cheap approach for modeling the interactions between convection and large-scale circulation. The configuration that is usually studied involves an interactive column, the dynamics of which is simulated by a cloud-resolving model or single-column model, coupled to a reference reservoir column (the reference-column approach; e.g., Raymond and Zeng 2005; Sobel et al. 2007; Sessions et al. 2010; Wang and Sobel 2011). The underlying assumption made is that the area of the interactive region to be simulated is very small in comparison with its surroundings, and thus, that it may be reasonable to neglect feedbacks to the state of the surroundings. Under the reference-column approach, the evolution of convection in a local region is fully coupled with the large-scale dynamics. However, the approach is not suitable for studying the influence on local convection of changes in remote convection.

Recently, Daleu et al. (2012) have extended the reference-column approach in order to allow two interacting columns to be fully coupled via a WTG-derived approximation of the large-scale circulation. In this coupled-column approach, the two columns are treated on an equal footing and their relative areas can take any value. The energy and moisture budgets of the system may be treated as open, allowing external source terms as in the reference-column approach, or else the budgets may be fully closed, as in the simulations of Daleu et al. (2012). In the limit of a large difference in column areas, Daleu et al. (2012) showed that the equilibrium state in the reference and coupled-column approaches agree well, at least for nonuniform surface conditions. However, for small or vanishing differences in surface conditions between the columns, there are qualitative differences between the two approaches that persist regardless of the relative sizes of the two columns. This result was attributed to the closed budgets in the coupled-column simulations.

The present study addresses the transition from suppressed to active convection over the tropical ocean, with a focus on the role of the large-scale circulation in modulating that transition. An important question is whether any qualitative differences occur in the rate or character of the transition process, when the transition is forced locally [via an increase in the sea surface temperature (SST), for instance] or remotely (via a change elsewhere that then affects the large-scale circulation experienced by the area in which convection was suppressed). This focus on the role of an interactive large-scale circulation, and on the comparison between local and remote mechanisms, means that the coupled-column approach is a natural choice of modeling framework, well suited to our objectives. Transitions that are forced by changes in the local surface conditions

have been investigated in various earlier studies (e.g., Sobel and Bretherton 2000; Khairoutdinov and Randall 2006; Kuang and Bretherton 2006; Wu et al. 2009), but the direct comparison against transitions forced by remote changes is a new feature of our study.

The starting point for our numerical experiments is a situation in which two distinct regions of the tropical atmosphere, with inhomogeneous surface conditions, are coupled through a large-scale circulation. The circulation will be expected to enhance convection in the ascending region and suppress it in the descending region. The inhomogeneity is then removed from the system by equalizing the SST between the regions. This is done by increasing SST in the suppressed-convection region, reducing SST in the enhanced-convection region, or a combination of both. We will examine the transient evolution of convection from a suppressed to a more active phase under the influence of a diminishing, and ultimately a vanishing, large-scale circulation.

This paper is organized as follows. Section 2 describes the model and our experimental setup and continues with the examination of the initial conditions used for the simulations of the transition. Section 3 presents and compares the main results of simulations that applied the locally, remotely, and locally and remotely forced transition methods. The transition from suppressed to active convection is quantified in section 4. The contributions of the large-scale circulation and surface forcing are decoupled in section 5, followed by a summary of the main findings in section 6.

2. Model description and experimental setup

a. The coupled-column model

Figure 1 illustrates the system considered in this study. It is a configuration representing two columns of tropical convection that are fully coupled via a large-scale circulation. The subscripts 1 and 2 are used to label the horizontal-domain-mean properties in columns 1 and 2, respectively; L is the length of the full system to be represented (i.e., of the two columns) and the individual column lengths are $L_1 = L_2 = L/2$.

The large-scale vertical velocities for columns 1 and 2 satisfy the following equation:

$$\overline{w}_2\frac{\partial\overline{\theta}_2}{\partial z}-\overline{w}_1\frac{\partial\overline{\theta}_1}{\partial z}=\frac{\overline{\theta}_2-\overline{\theta}_1}{\tau}. \qquad (1)$$

Separate expressions for $\overline{w}_1$ and $\overline{w}_2$ are then easily obtained by applying the two-column form of the mass continuity equation:

$$\overline{w}_1+\overline{w}_2=0. \qquad (2)$$

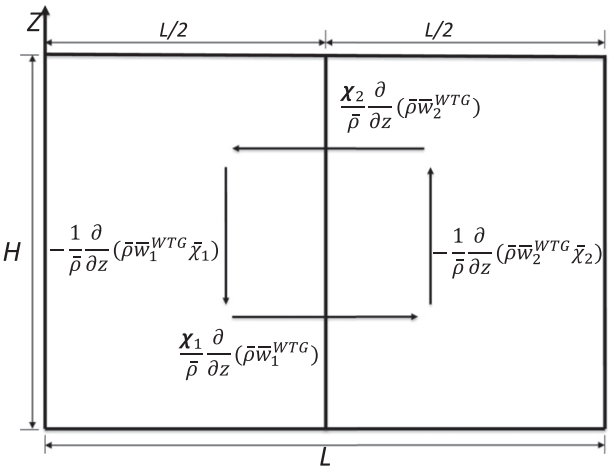

FIG. 1. Schematic of the two-column model. The arrows show the direction of the flow and the text indicates the transport terms associated with the flow. The variable χ represents potential temperature or specific humidity of water vapor.

The WTG approach breaks down in the boundary layer (Sobel and Bretherton 2000). Here we choose a nominal boundary layer top of 1.5 km, and for $z <$ 1.5 km, we obtain the WTG vertical velocity by interpolating linearly in height between the value at the first model level above 1.5 km to a prescribed value of zero at the surface. The variables $\overline{w}_1$ and $\overline{w}_2$ are then used to compute the large-scale advective tendencies of heat and moisture between the two columns. The change in the horizontal column-mean quantity $\overline{\chi}$ due to the derived large-scale circulation is written in flux form as

$$\frac{\partial\overline{\chi}}{\partial t}+\nabla_h\cdot(\mathbf{v}^{\mathrm{WTG}}\overline{\chi})+\frac{1}{\overline{\rho}}\frac{\partial}{\partial z}(\overline{\rho w}^{\mathrm{WTG}}\overline{\chi})=0. \qquad (3)$$

The second and third terms on the left-hand side of Eq. (3) represent the horizontal and vertical transport by the large-scale circulation, respectively. At each model level, we assume that the horizontal flow $\mathbf{v}^{\mathrm{WTG}}$ is either all into or all out of each column. We use the continuity equation to express the horizontal transport as a function of a vertical derivative, and we use an upwind advection scheme to calculate the tendency of $\overline{\chi}_1$ due to the derived large-scale circulation,

$$\left(\frac{\partial\overline{\chi}_1}{\partial t}\right)_{\mathrm{WTG}}=\frac{\chi_*}{\overline{\rho}}\frac{\partial}{\partial z}(\overline{\rho w}_1^{\mathrm{WTG}})-\frac{1}{\overline{\rho}}\frac{\partial}{\partial z}(\overline{\rho w}_1^{\mathrm{WTG}}\overline{\chi}_1), \qquad (4)$$

and similarly for $\overline{\chi}_2$. Here χ_* is the appropriate upwind value of $\overline{\chi}$ and the vertical derivative is calculated using an upwind scheme. Equation (4) is applied to potential temperature and water vapor only and does not apply to

any form of hydrometeor. Full derivations of the large-scale transport tendency terms are given in Daleu et al. (2012).

The WTG calculations are performed on a coupling time step dt_{WTG} of 10 min. This choice is essentially arbitrary and, in particular, there is no significant variation in the equilibrium-mean rain rates for values of dt_{WTG} ranging between 0.5 and 30 min (Daleu et al. 2012).

The large-scale circulation that is derived from Eq. (1) acts to keep the column-mean potential temperature profiles of the two columns close to each other. This formulation of the large-scale circulation relies on the physical principle that over a large area of the tropical free troposphere, the large-scale horizontal gradients and time tendencies of temperature are small because gravity waves rapidly redistribute buoyancy anomalies toward nearly uniform density on isobaric surfaces. Hence, the time scale τ in Eq. (1) can be thought of as being related to the time for gravity waves to propagate across the system and so is related to the size of the system.

The approach that is briefly described above allows two interacting columns to be coupled via the WTG approximation. In this study, the convective properties in each column are determined from an embedded CRM. We use a CRM that is based on version 2.4 of the Met Office Large-Eddy Model (LEM; Shutts and Gray 1994; Petch and Gray 2001). The model has a five-category prognostic microphysical scheme (Swann 1998; Brown and Heymsfield 2001) with prognostic variables for the mixing ratios of water vapor, cloud water, rain, ice, graupel, and snow and for the number concentration of ice. The reader is referred to Gray et al. (2001) for further details.

The configuration of the CRM is similar to that described by Daleu et al. (2012), which is a two-dimensional (2D) configuration with the domain width of 128 km and the model top placed at about 20 km. This domain size is sufficient to accommodate an ensemble of convective clouds, and it is sufficient for examining the transient evolution of convection and the associated transport terms during the transition from a suppressed to a more active phase of convection and vice versa. An advantage of using a 2D CRM is that it is computationally cheap to run compared to the three-dimensional (3D) CRM. Hence, a large number of simulations can be performed in order to obtain an ensemble-mean behavior or in order to test different mechanisms involved in the transition and to assess sensitivity. As far as the equilibrium properties of convective ensembles are concerned, past studies (Tompkins 2000; Redelsperger et al. 2000) show that the results of 2D CRMs are comparable with those from 3D CRMs.

There are 60 levels in the vertical, on a stretched grid with finer resolution closer to the surface. The mid-tropospheric grid spacing is about 330 m and the horizontal grid spacing is 500 m. The lateral boundary conditions are periodic for all prognostic variables. The lower boundary is an ocean surface, with a roughness length of 2×10^{-4} m and a prescribed spatially uniform SST. The top and bottom of the domain are rigid lids. A sponge layer is placed in the upper one-fourth of the domain (from 15 to 20 km) to prevent vertically propagating gravity waves from being reflected back into the domain.

In this study, the cooling of the column due to outgoing longwave radiation is prescribed as being a horizontally homogeneous and noninteractive value through the troposphere. The value is 1.5 K day^{-1} up to 220 hPa and then decreases linearly in pressure to reach the value of 0 K day^{-1} at about 120 hPa. The wind along the domain is relaxed to zero in order to prevent the development of along-domain wind shear that may otherwise occur in 2D simulations (Tompkins 2000; Mapes and Wu 2001) and that would encourage the formation of squall lines (e.g., Rotunno et al. 1988; Robe and Emanuel 2001; Tao et al. 1999). The wind across the domain is relaxed to 5 m s^{-1} with a relaxation time scale of 2 h. This value of wind speed affects the simulations via the bulk aerodynamic formulas that are used to compute surface fluxes. As a result, surface evaporation is increased compared to the no-wind value.

b. *Experimental setup*

Idealized simulations of a gradually forced transition from a suppressed to a more active phase of convection are performed by adopting the strategy described below.

1) Run the coupled-column model to equilibrium with nonuniform SST.
2) Use the instantaneous states at equilibrium of the above simulations as a set of initial conditions for the simulations of the transition.
3) Force the column with suppressed convection to undergo the transition to a more active phase of convection by changing the SSTs toward uniform values across the columns. The transition has been forced in three different ways: (i) the locally forced transition that is conducted by increasing the value of SST in the column with suppressed convection, (ii) the remotely forced transition that is conducted by decreasing the value of SST in the column with enhanced convection, and (iii) the locally and remotely forced transition that is conducted by increasing the value of SST in the column with suppressed convection while simultaneously

TABLE 1. Values of SST (K) for columns 1 and 2. The simulations are performed with columns of equal areas and with $\tau = 2$ h.

	Experiment		
	C	M	W
SST_1	300.7	301.7	302.7
SST_2	302.7	303.7	304.7

decreasing the value of SST in the column with enhanced convection.

4) Finally, examine the transient response of convection to the change in SST and to the resulting change in the strength of the WTG-derived large-scale circulation.

Alternatively, the simulations of the transition can be initialized from coupled-column simulations over nonuniform surface wind speed and the transition to a more active phase of convection can be forced in the column with suppressed convection by changing the surface wind speeds toward uniform values across the columns. However, results from changing the surface wind speed were found to be broadly similar to those from changing the SST, and hence, only the results from changing the SST will be discussed here.

c. *Initial conditions*

Three simulations are performed under the coupled-column approach with the SST difference of 2 K between the columns. In each of these simulations, column 1 is chosen to be colder than column 2 (Table 1); the WTG coupling time scale τ is equal to 2 h; and the columns have equal areas, thus $w_2 = -w_1$ [see Eq. (2)]. Each column is initialized with the mean profiles obtained in a previous radiative–convective equilibrium (RCE) simulation performed with the SST equal to the value in that column. Each simulation is run for 40 days and an average over the last 20 days is used to define the state and statistics of the model at equilibrium with the WTG-derived large-scale circulation. These three simulations have different values of mean SST. They are classified as C, M, and W for cold, medium, and warm, respectively.

For each simulation, the absolute difference in SST drives an overturning circulation with its ascending branch being in column 2 and the enhanced precipitation there balancing the reduction in precipitation in column 1. To analyze the quasi-equilibrium state achieved for simulations listed in Table 1, we first consider Fig. 2, which shows the profiles at equilibrium of temperature and specific humidity for columns 1 and 2 of the coupled-column system classified as M. In the free troposphere, the WTG-derived circulation keeps the temperature profiles close to each other. The WTG calculations are not applied in the boundary layer, although the large-scale circulation does exist there (section 2a). As a result, the horizontal temperature difference is relatively greater in the boundary layer compared to the free troposphere, where the maximum value is 0.3 K at the levels where the latent heat released is also maximal. This value is relatively small compared to the value of up to 3.5 K obtained in the RCE simulations of the CRM with 1 K difference in SST (Daleu et al. 2012) and compared to the value of up to 3 K obtained in the RCE simulations of a single-column model with 1 K difference in SST (Ramsay and Sobel 2011).

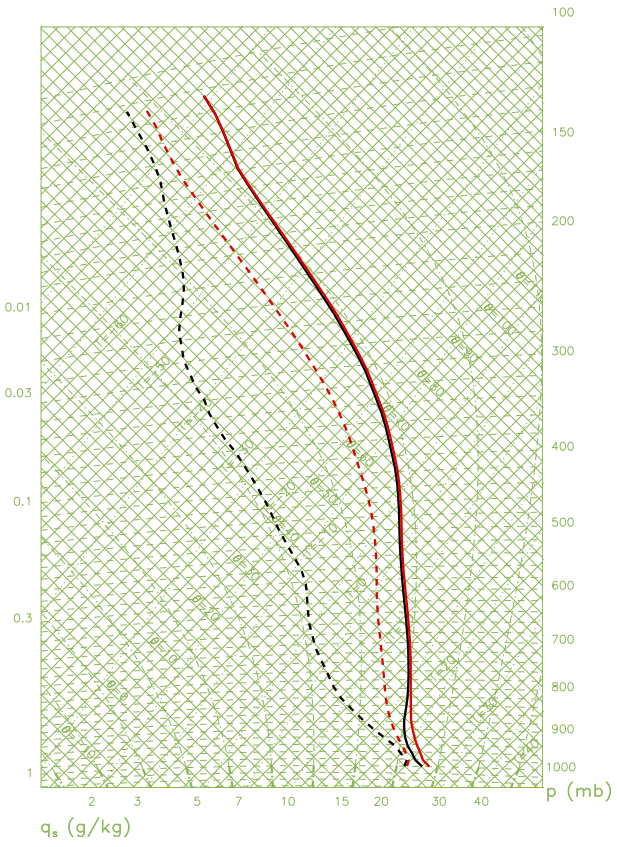

FIG. 2. Domain-mean profiles at equilibrium of temperature (solid curves) and specific humidity (dashed curves) plotted on a tephigram. The profiles are for column 1 (black curves) and column 2 (red curves) of the coupled-column system classified as M.

On the other hand, the drying and warming effects from the descending branch of the large-scale circulation inhibit convection in column 1 while the cooling and moistening effects from the ascending branch of the large-scale circulation enhance convection in column 2. As a result, column 1 becomes relatively dry (dominated by shallow convection) while column 2 becomes relatively moist compared to their RCE states.

We also consider Fig. 3, which shows the domain-mean potential temperature and specific humidity tendency profiles at equilibrium for columns 1 and 2 of the coupled-column system classified as M. At each level, the total changes are close to zero, as expected for equilibrium.

Note that the mean states achieved at equilibrium in the three simulations C, M, and W are very similar for the whole domain. In addition, mean statistics are very similar. For instance, the mean rain rates and surface evaporation rates agree to within 0.3 mm day^{-1}. The mean rain rate in column 1 is decreased by 79% (now 0.98 mm day^{-1}) relative to the mean rain rate of about 4.78 mm day^{-1} obtained in the RCE simulations with various values of SST. The mean rain rate in column 2 is increased to 8.47 mm day^{-1} in order to maintain the energy balance of the whole system. The values of surface evaporation are 3.48 and 6.04 mm day^{-1} for columns 1 and 2, respectively. The excess of evaporation over precipitation in column 1 and the deficit of evaporation over precipitation in column 2 are balanced by the large-scale circulation that advects moisture from column 1 to column 2.

Figure 4 shows the large-scale mass flux profiles at equilibrium for column 1 in the coupled-column simulations listed in Table 1. The large-scale mass flux is computed as the product of density and the WTG vertical velocity. With the columns having equal areas, the large-scale mass flux profiles at equilibrium for column 2 are the mirror images of the profiles presented in Fig. 4. In this study, the large-scale mass fluxes are top heavy as a result of the low static stability in the upper troposphere (Daleu et al. 2012). A similar result was obtained in other simulations of the interactions between convection and the large-scale circulation that is parameterized using the WTG approach; however, simulations in which convection is coupled to a large-scale gravity wave of specified horizontal wavelength (damped gravity wave approach) produce mass fluxes that are less top heavy (e.g., Kuang 2012; Wang et al. 2013).

The mean states and statistics, in addition to the strength and the vertical structure of the large-scale circulation at equilibrium, do not depend on the actual SST in each of the coupled columns. Rather, they depend only on the SST difference between the two columns. This is an important point for the transition experiments because it allows various experiments to be compared, despite the fact that they start from different values of the mean SST in the system.

3. Results

In each of the simulations described above, the large-scale circulation that develops in the system suppresses convection in column 1 relative to column 2 and relative to the convective state achieved in the equivalent RCE simulation. In this section, we examine the evolution of clouds and transport statistics of the simulations in which convection in column 1 is forced to undergo the transition to a more active phase by applying the locally, the remotely, or the locally and remotely forced transition methods. Table 2 presents the values of SSTs for columns 1 and 2 at the beginning and at the end of each simulation of the transition.

a. *Locally forced transition*

In this section, the simulation of the transition from suppressed to active convection is conducted with the initial conditions taken from instantaneous profiles at equilibrium of the simulation C. Column 1 is forced to undergo the transition by increasing the SST in column 1 to match the value in column 2 over the course of 1 day. This is an example of simulated transition that is driven by a change in the underlying SST and by the induced change in the strength of the large-scale circulation.

The simulation is run for 40 days after the start of the SST transition. Ensemble-mean results are obtained by averaging the results of five realizations, which in this study are differentiated by the time at which the transition is initialized. As discussed above, an equilibrium simulation is used to provide initial conditions for the transition experiments, and ensemble states are started at intervals of 2 days to provide different starting conditions. Ensemble averages of the transition are made by considering the start of the SST change to be time 0. The time evolution of some fields (e.g., precipitation) exhibits high-frequency variability that may partly be due to the 2D domain used, as first noted by Grabowski et al. (1998). Hence, the ensemble averages are applied to provide a smoother version of features that are also evident in individual realizations. This set of ensemble realizations of a locally forced transition will be henceforth be referred to as experiment 1.

Figures 5 and 6 present the temporal evolution of column-integrated heating and moistening rates from the large-scale circulation and the temporal evolution of surface evaporation and rain rates, respectively. The results are the 5-day running mean and ensemble mean for columns 1 and 2 of experiment 1 (solid curves). We expressed the heating rates in millimeters per day via the latent heat constant in order to allow easy comparison with the evaporation and precipitation rates. The simulation of the transition starts at day 0. Hence, results presented for days before the SST is changed are those of the simulation C. As already discussed in section 2c, before the SST is changed, surface evaporation and rain rates are reduced in column 1 and enhanced in column 2

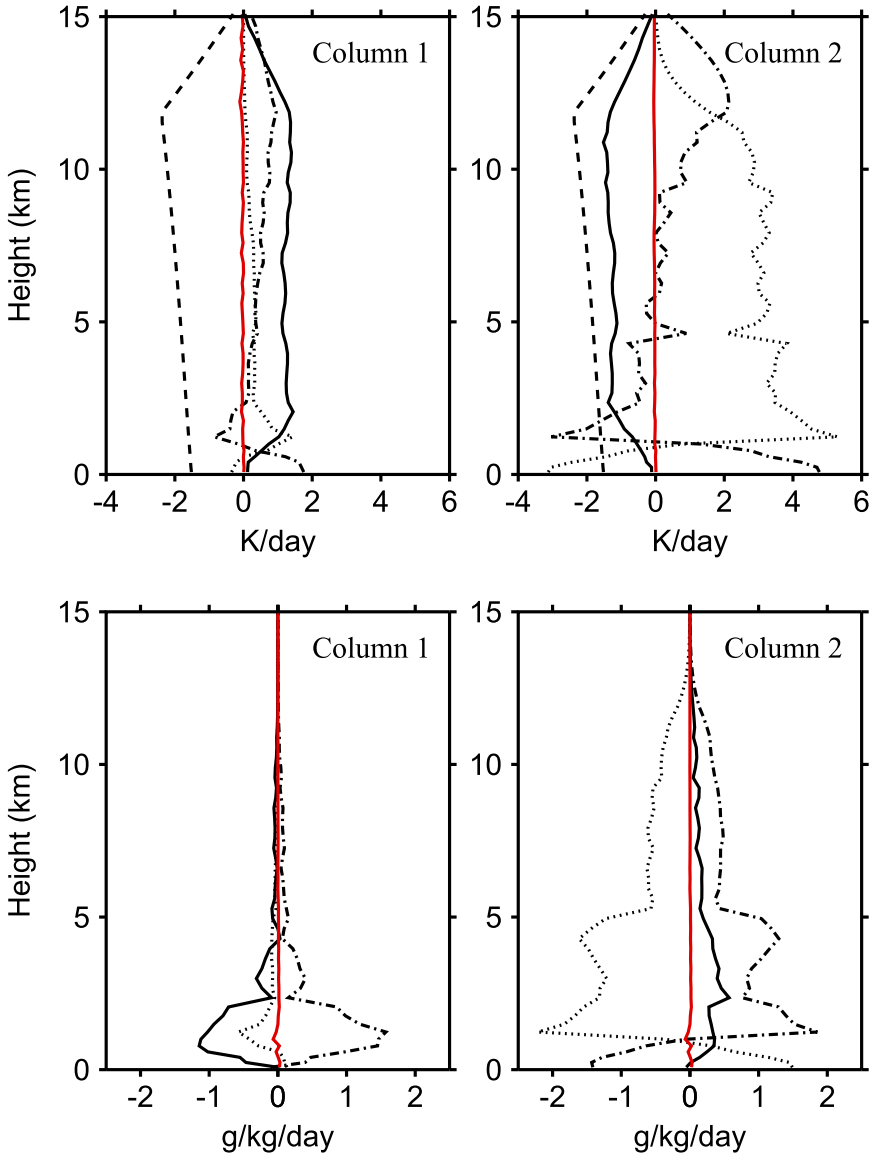

FIG. 3. Domain-mean (top) potential temperature and (bottom) specific humidity tendency profiles at equilibrium. The profiles are for (left) column 1 and (right) column 2 of the coupled-column system classified as M. The total change (solid red curves) is defined as the sum of tendencies due to the WTG-derived large-scale circulation (solid black curves), microphysics (dotted curves), and advection as simulated directly in the CRM (dash–dotted curves). In addition, there is a tendency due to radiation (dashed curves) in the potential temperature.

in response to the diagnosed large-scale circulation that advects moisture from column 1 to column 2. From day 0, the SST in column 1 is increased at the rate of $2\,\mathrm{K\,day^{-1}}$ until day 1, when it reaches the value in column 2. The change in SST produces a change in the strength of the large-scale circulation. The large-scale circulation decreases rapidly over the first 8 days, followed by a much slower decrease. Over a long period of integration, the columns adjust toward a final equilibrium state with no time-mean large-scale circulation and with the mean states and statistics very similar to those obtained in the RCE simulation with an SST of 302.7 K (Daleu et al. 2012).

Surface evaporation in column 2 decreases slowly toward the RCE value. However, surface evaporation in column 1 overshoots in response to the increase in the underlying SST before decreasing slowly toward the RCE value. Over days 0–7, the rain rate in column 1

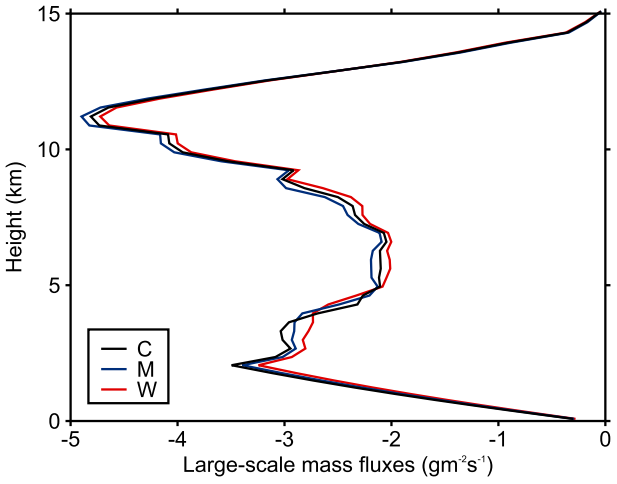

FIG. 4. Profiles of large-scale mass flux, which is computed as the product of density and the WTG vertical velocity. The profiles are for column 1 in the simulations listed in Table 1.

increases rapidly before evolving more slowly and recovers the RCE value by day 25. From the consideration of energy balance of the coupled-column system, the natural effect of an increase in rain rate in column 1 is a corresponding reduction in rain rate in column 2.

Column-integrated values hide information on the vertical structure. Figure 7 presents time–height cross sections of heating rates from the derived large-scale circulation, domain-mean relative humidity, and domain-mean heating rates from microphysics. The results presented are for column 1 of experiment 1.

From day 0, surface evaporation is increased into column 1 and hence into the system as a whole. Convective cells in column 1 become more active. However, column 1 is initially dry, and these cells quickly lose buoyancy because of the entrainment of dry environmental air. As a result, the first apparent changes in the vertical structure of convection are delayed until day 2. After day 1, the SST in column 1 is equal to the value in column 2. The large-scale circulation is not switched off instantaneously. Rather, its strength reduces and reaches a value very close to zero over a period of about 20 days. For comparison, we performed an experiment in which the SST in column 1 is increased as in experiment 1, but the heating and moistening rates from the WTG-derived large-scale circulation are not applied from day 0. The temporal evolution of rain rates in column 1 of that experiment is shown by the dashed curve in the bottom-left panel of Fig. 6. When compared to the temporal evolution of rain rates in column 1 of experiment 1 (solid curve in the bottom-left panel of Fig. 6), it clearly demonstrates that temperature and humidity perturbations resulting from the large-scale circulation affect the convection. As a result, the transition

TABLE 2. Values of SST (K) for columns 1 and 2 before the SST is changed and at the end of simulations for experiments that apply the locally, remotely, and locally and remotely forced transitions methods.

	Experiment		
	1	2	3
Method	Local forcing	Remote forcing	Local and remote forcing
SST_{i_1}	300.7	302.7	301.7
SST_{i_2}	302.7	304.7	303.7
SST_{f_1}	302.7	302.7	302.7
SST_{f_2}	302.7	302.7	302.7

to deep convection under the influence of an evolving large-scale circulation is delayed compared to an experiment that does not apply the heating and moistening rates from the WTG-derived large-scale circulation from day 0.

As the large-scale circulation is reduced, enhanced evaporation is maintained in column 1 so that moisture is recharged in the free troposphere and convective cells deepen accordingly. Shortly after day 2, more convective clouds are able to grow past the layer of intermediate clouds around the freezing level located at about 5 km. Shortly after day 3, the large-scale circulation is rapidly reduced in the free troposphere. As a result, convective cells are able to emerge with cloud tops as high as the tropopause level. From day 8, very little large-scale circulation remains in the whole troposphere and the column is sufficiently moist to sustain active convection with properties close to those in the final equilibrium state. In this experiment, column 1 moves from a state with suppressed convection to a state with substantial deep convection over a period of about 8 days.

Figure 8 compares soundings at four different times during the transition period in column 1. From the initial state, the thermodynamic soundings have a considerable amount of convective available potential energy (CAPE) for an undiluted parcel to rise from the near surface to the upper troposphere (the dash–dotted lines in Fig. 8). The CAPE increases from 1323 J kg^{-1} before the SST is changed to the mean value of 1958 J kg^{-1} obtained by averaging over days 30–40. At day 0, there is an inversion at about 900 hPa, where the boundary layer with temperature tied to the surface temperature of 300.7 K meets the free troposphere with temperature constrained to remain close to the profile in column 2. This inversion caps convection and, despite the important amount of CAPE, convective cells that succeed to go beyond the boundary layer entrain the dry air from their surroundings and quickly lose buoyancy.

At day 2 the SST in column 1 is 2 K warmer than its value at day 0, but the large-scale circulation remains for several days. As a result, convective cells that become active are not able to develop or penetrate above 3 km

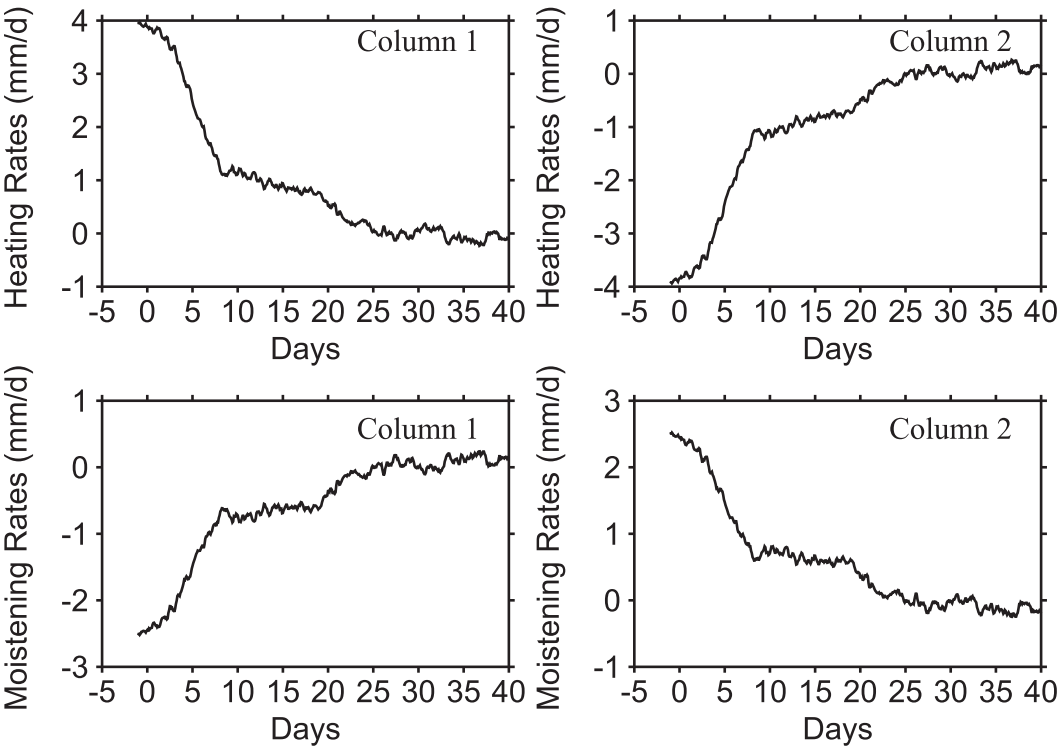

FIG. 5. Time evolution of column-integrated (top) heating and (bottom) moistening rates from the large-scale circulation. The results are the 5-day running mean and ensemble mean for (left) column 1 and (right) column 2 of experiment 1.

until day 3. Hence, the availability of positive energy at high levels is not by itself sufficient to prevent the large-scale descent from inhibiting convection. As the large-scale circulation is reduced, the midtropospheric moisture is recharged favoring further development of convection. The increase in moisture in the free troposphere increases convective rainfall (Fig. 6), but the transition from suppressed to more active convection is not complete until the middle troposphere is sufficiently moistened. The inversion located at about 900 hPa at day 0 is eroded as convection becomes more active and deepens. From day 6, the inversion is no longer apparent. Between days 3 and 6, significant changes occur to the CAPE and tropospheric moisture. During this period, a transition to deep convection occurs as soon as the middle troposphere becomes moist enough for the column to be able to support and sustain convection with properties similar to those obtained in the RCE simulation with an SST of 302.7 K.

b. *Remotely forced transition*

Section 3a discussed the results of an experiment in which the transition from suppressed to active convection is forced locally. In this section, we show the results of an experiment in which the transition is forced remotely. This experiment is an ensemble of five simulations of the transition that are initialized from five instantaneous states at equilibrium of the simulation W. For each simulation, the large-scale circulation is reduced in the system by decreasing the SST in column 2 to the value in column 1 over the course of 1 day. This is an example of the transition being driven by a change in the large-scale circulation that is caused by a remote change in SST. This experiment will henceforth be referred to as experiment 2.

Note that in contrast to experiment 1, to reach the final equilibrium state, moist static energy must be removed from column 2 of experiment 2 and hence from the system as a whole. Thus, the complete system in experiment 2 cools and dries while the system in experiment 1 warms and moistens. However, experiments 1 and 2 have the same value of mean SST at the end of the integrations, that is, 302.7 K. As a result, experiments 1 and 2 reach a very similar equilibrium state, which in turn is very similar to the state obtained in the RCE simulation of the uncoupled CRM with an SST of 302.7 K (results not shown).

We now compare the evolution of the lowest 2 km in column 1 of experiment 1 to that in column 1 of experiment 2. We consider Fig. 9, which shows the deviation of the ensemble-mean profiles in column 1 of experiments 1 and 2 from the RCE profiles of potential

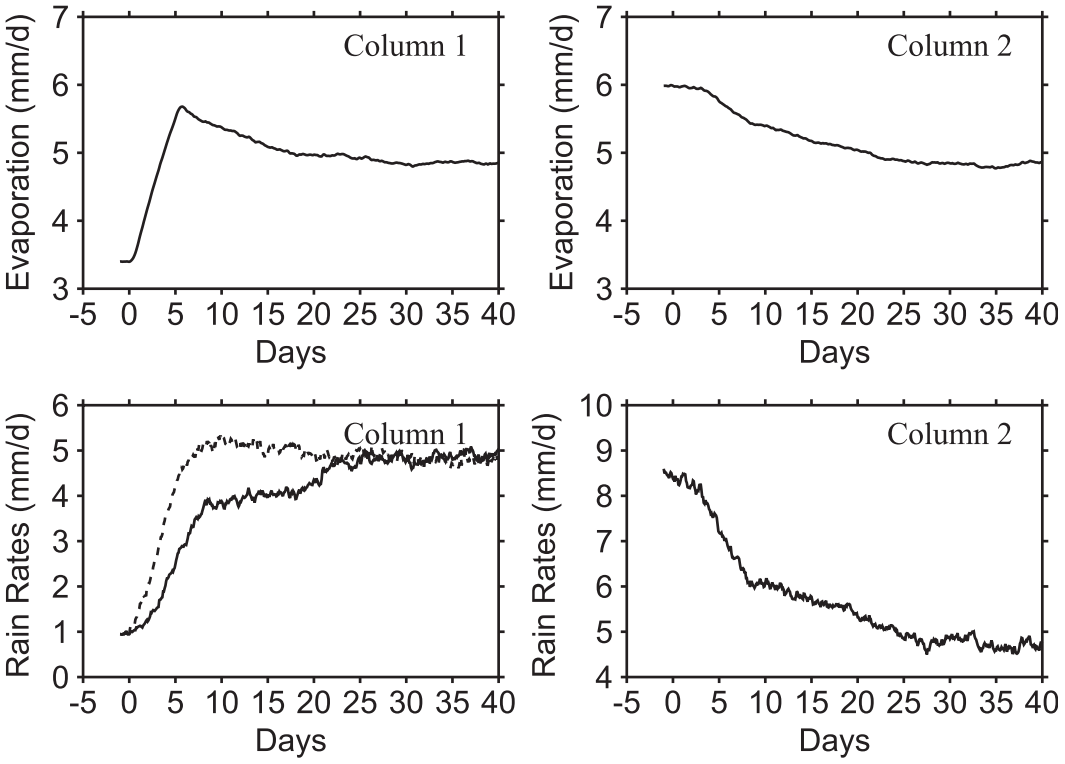

FIG. 6. Time evolution of (top) surface evaporation and (bottom) rain rates. The results are the 5-day running mean and ensemble mean for (left) column 1 and (right) column 2 of experiment 1. The dashed curve represents the 5-day-running-mean and ensemble-mean rain rates for column 1 of an experiment that applies the local forcing and does not apply the heating and moistening rates from the WTG-derived large-scale circulation from day 0.

temperature and specific humidity of the uncoupled CRM with an SST of 302.7 K. When the SST of a column is increased, surface evaporation increases, shallow convection becomes more active, and the boundary layer warms and moistens. On the other hand, when the SST of a column is decreased, convection is inhibited and the boundary layer cools and dries. Such effects do not occur directly in column 1 of experiment 2, since its SST is not changed. As a result, over the course of 3 days, the values of the potential temperature below 500 m are increased by 1.5 K in column 1 of experiment 1 compared to a reduction of only 0.1 K in column 1 of experiment 2. However, over the same period the values of potential temperature above 1 km are increased by about 0.1 K in column 1 of experiment 1 compared to a mean decrease of about 0.7 K in column 1 of experiment 2. Hence, the static stability decreases rapidly in column 1 of experiment 1 relative to column 1 of experiment 2, suggesting that convection develops and grows more easily within column 1 of experiment 1 relative to column 1 of experiment 2.

We now examine the evolution of specific humidity. During the first 2 days, results for the moisture transport by convection (result not shown) reveal that in column 1 of experiment 1 shallow convection transports an important amount of moisture (compared to the moisture transport by convection in column 1 of experiment 2, in which the SST is not increased) from the surface to the upper levels. During the same period, the strength of the large-scale circulation is not very different than that at day 0 (see Fig. 7, top left). The moisture transport out of column 1 by the large-scale circulation in addition to the moisture transport out of the boundary layer by convection is more than enough to balance the increase in surface evaporation that is caused by the increase in the underlying SST. This point enables strong evaporation to be maintained. As a result, the moisture in the near-surface portion of column 1 of experiment 1 is slightly reduced relative to the moisture at day 0. From day 3, the large-scale circulation weakens and the specific humidity in the whole column increases toward the equilibrium state. However, from day 0, column 1 of experiment 2 is relatively moist below 0.9 km and relatively dry above 0.9 km compared to the equilibrium profile. As the large-scale circulation is removed from the system, the moisture adjusts toward the equilibrium profile in a very simple fashion, by drying below 0.9 km and moistening above.

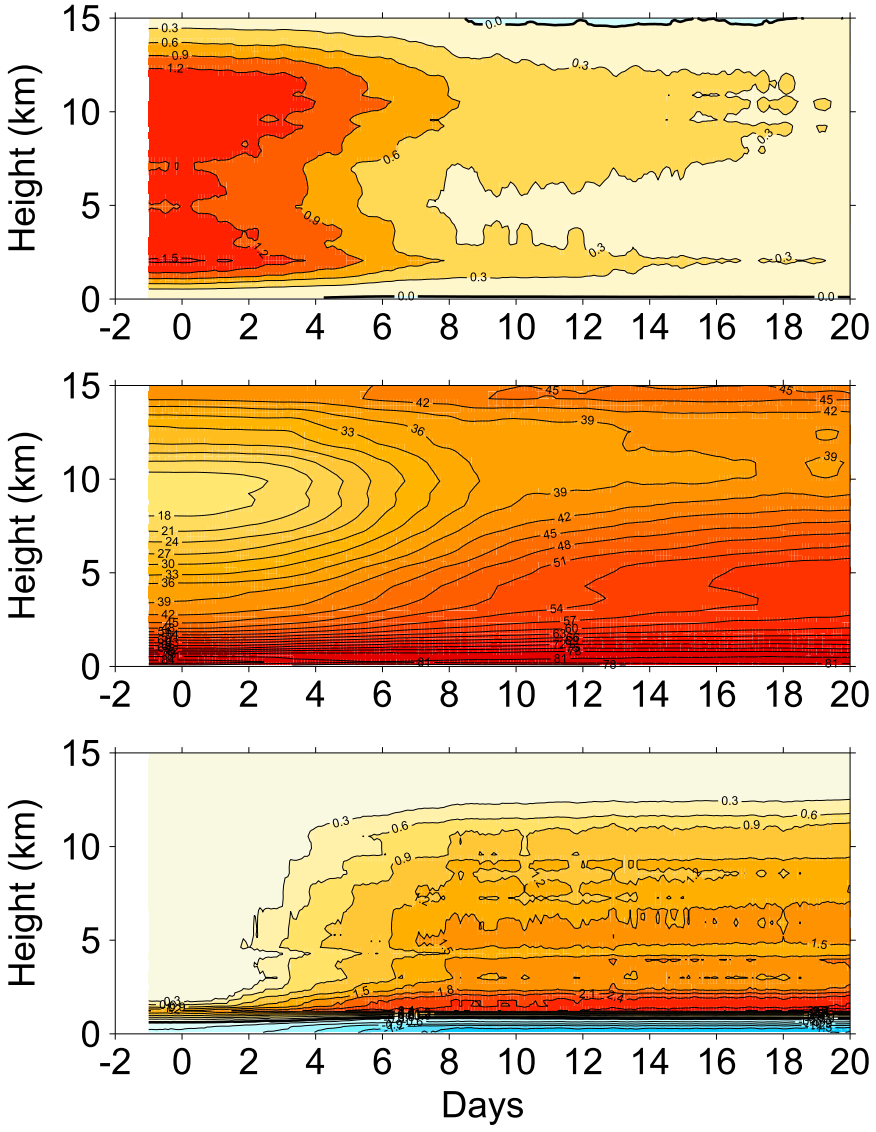

FIG. 7. Time–height cross sections of heating rates from the (top) derived large-scale circulation, (middle) domain-mean relative humidity, and (bottom) domain-mean heating rates from microphysics. The profiles are the 5-day running mean and ensemble mean for column 1 of experiment 1. The contour intervals are 0.3 K day^{-1} in the top and bottom panels and 3% in the middle panel.

Figure 10 presents the time–height cross sections of heating rates from the large-scale circulation and from microphysics. These results are for column 1 of experiment 2. They can be directly compared to the top and bottom panels of Fig. 7, which show the corresponding results for column 1 of experiment 1.

As discussed above, the first change in the vertical structure of convection is delayed in column 1 of experiment 2 relative to column 1 of experiment 1. It appears at day 4. This delay is reflected in all of the diagnostic fields examined. For instance, the large-scale circulation lasts longer in the upper troposphere of experiment 2. As a result, the transition period is extended until day 14 in column 1 of experiment 2 compared to day 8 in column 1 of experiment 1.

c. *Locally and remotely forced transition*

In this section, we show the ensemble-mean results of five simulations of a transition initialized from five instantaneous states at equilibrium of the simulation M. For each simulation, the transition is forced by increasing the SST in column 1 while simultaneously

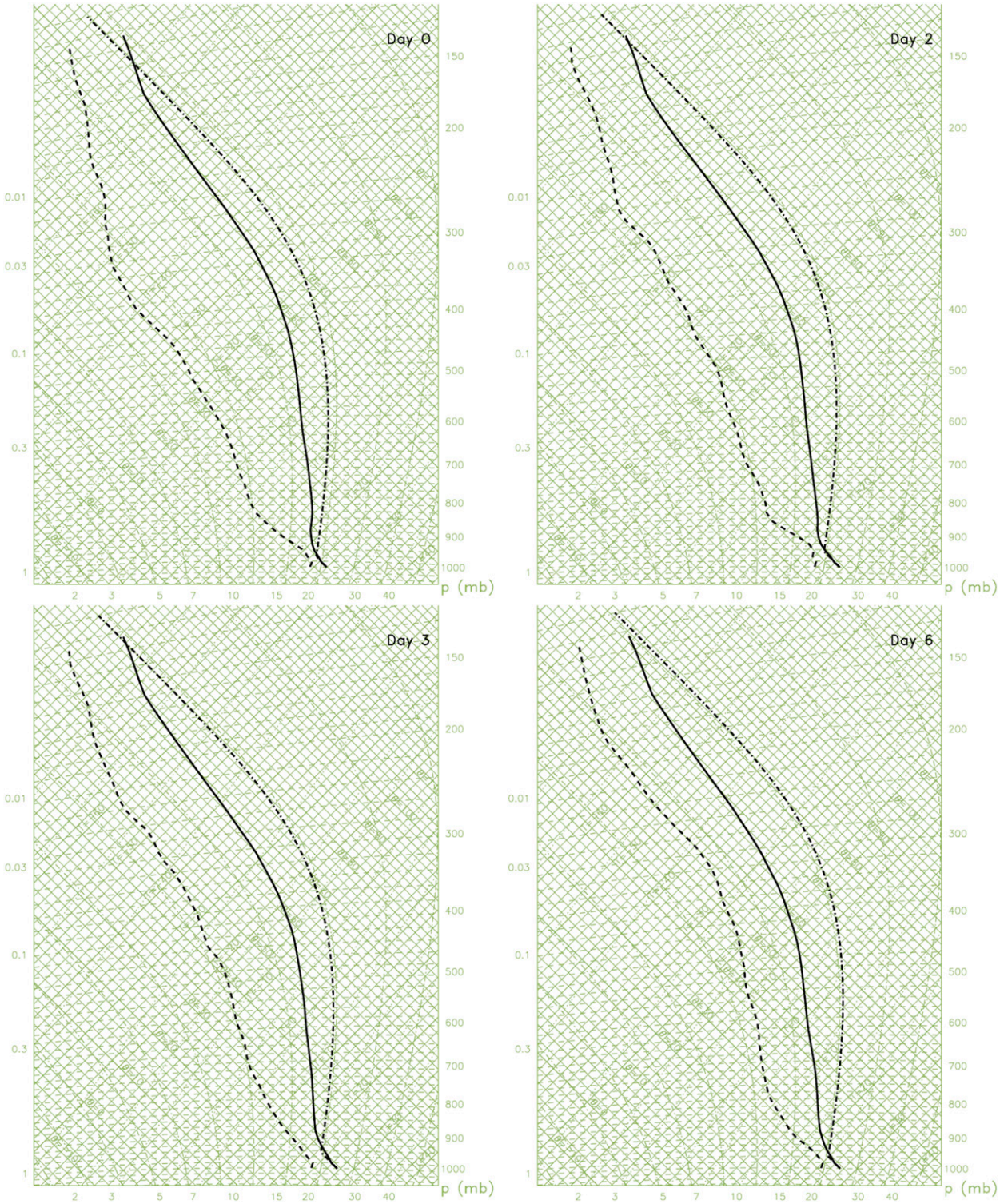

FIG. 8. Temperature and specific humidity profiles for column 1 of experiment 1. The profiles are plotted at (top left) day 0, (top right) day 2, (bottom left) day 3, and (bottom right) day 6.

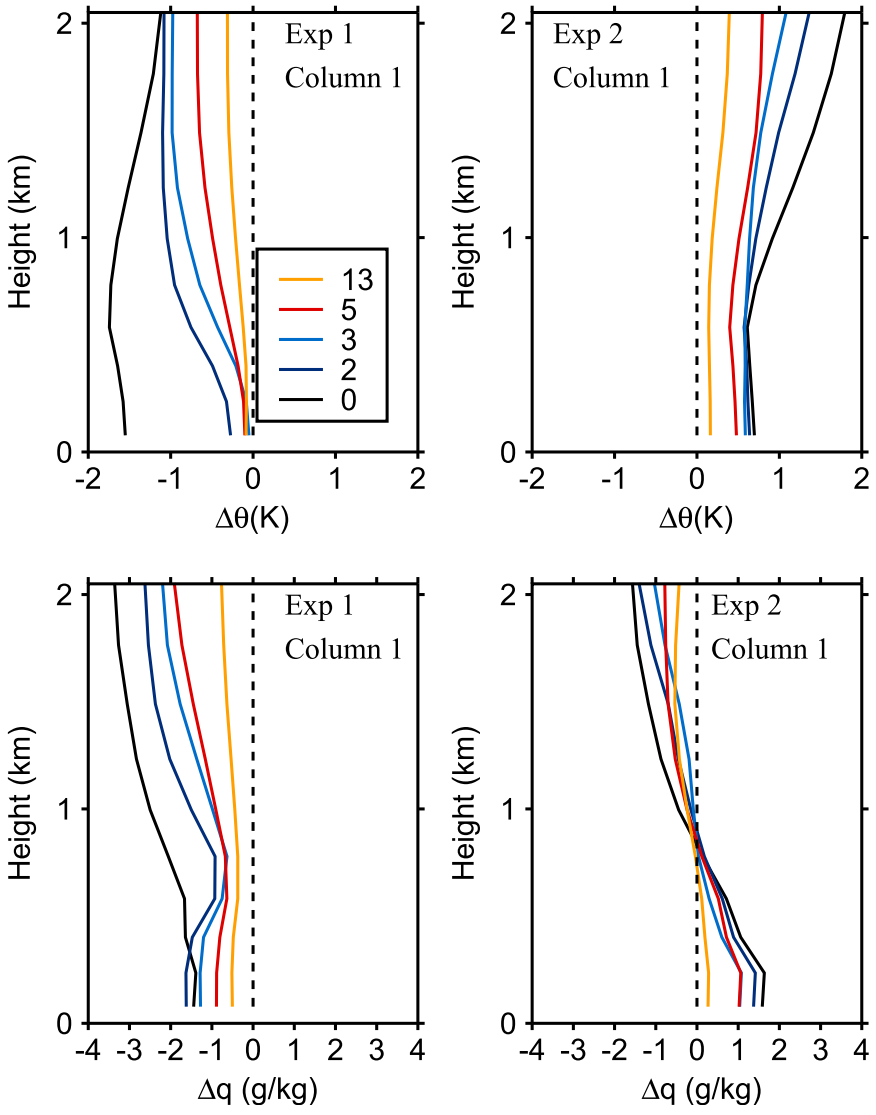

FIG. 9. Deviations from the RCE profiles of (top) potential temperature and (bottom) specific humidity of the uncoupled CRM with an SST of 302.7 K. The deviations are plotted for the ensemble-mean profiles in column 1 of (left) experiment 1 and (right) experiment 2. The deviations from RCE are shown for the average over the day before the SST is changed (black curves), over days 1–2 (dark blue curves), days 2–3 (light blue curves), days 4–5 (red curves), and days 12–13 (yellow curves). The results are plotted for the lowest 2 km only.

decreasing the SST in column 2 so as to obtain the same value of 302.7 K in each of the columns over the course of 1 day. Thus, the transition from suppressed to active convection is forced by both local and remote changes. This ensemble of realizations will henceforth be referred to as experiment 3.

Figure 11 compares the temporal evolution of surface evaporation and rain rates for columns 1 and 2 in experiments 1–3. In all three experiments, the changes in SSTs result in no time-mean large-scale circulation in the system after 20 days or so, and the final equilibrium state achieved is very close to that achieved in the equivalent RCE simulation with an SST of 302.7 K.

The changes in SSTs influence surface evaporation. Surface evaporation in a column with unaltered SST adjusts slowly toward the RCE value while surface evaporation in a column directly subjected to an SST change overshoots and then adjusts slowly toward the RCE value. Precipitation changes are monotonic and increase in column 1 and decrease in column 2 as the large-scale circulation is reduced.

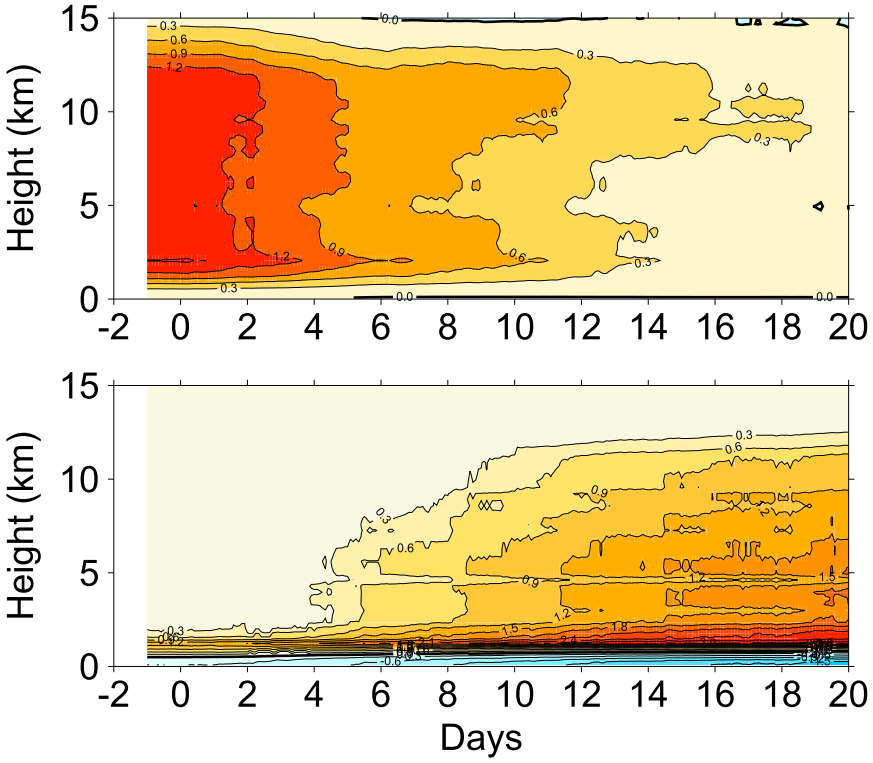

FIG. 10. Time–height cross sections of heating rates from the (top) derived large-scale circulation and (bottom) domain-mean heating rates from microphysics. The profiles are the 5-day running mean and ensemble mean for column 1 of experiment 2. The contour interval is 0.3 K day^{-1}.

The time–height cross sections of heating rates from the large-scale circulation and the domain-mean heating rates from microphysics in column 1 of experiment 3 (results not shown) reveal that the first change in the vertical structure of convection is delayed relative to experiment 1 but is advanced relative to experiment 2. Nevertheless, the common feature of all these simulations is that as the strength of the large-scale circulation decreases, moisture is recharged into the dry column and convection deepens accordingly.

Experiments 1–3 illustrate three different methods of forcing the transition in column 1. Our discussions have assumed that differences in the results indicate a dependency on the methods of forcing the transition but that is not necessarily the case. An alternative explanation could be that the differences occur because of different values of the mean SST at day 0. We have checked on this by investigating separately the sensitivity to the mean SST. For example, results obtained for experiment 2 are broadly similar to those obtained from another set of remotely forced simulations of the transition that are initialized from the simulation C. For full details, see Daleu (2013). Hence, the transition to active convection is insensitive to the initial mean SST.

4. The transition time

To summarize the evolution of column 1 from a state with suppressed convection to a state with more active convection and its dependency to the forcing mechanism, it is convenient to introduce a transition time t^*. Here, t^* is defined based on the increase of the rain rate (RR).

The temporal evolution of RR for column 1 in experiments 1–3 is presented in Fig. 12. The range of the five ensemble realizations is also shown. Note that for all the simulations performed in this study, the variability in precipitation between the ensemble members is similar to that shown in this figure, while the variability in evaporation is very small.

Before the SST is changed, rain rates produced in all the simulations listed in Table 1 are very close. They evolve at different rates between days 4 and 12, reflecting the different processes responsible for moistening the column.

Since the final equilibrium state achieved in experiments 1–3 is known to be the RCE state at 302.7 K, it is reasonable to define t^* based on the rain rate deficit (RR_d) in column 1. This is calculated as

$$RR_d = RR_{RCE} - RR(t < 0), \quad (5)$$

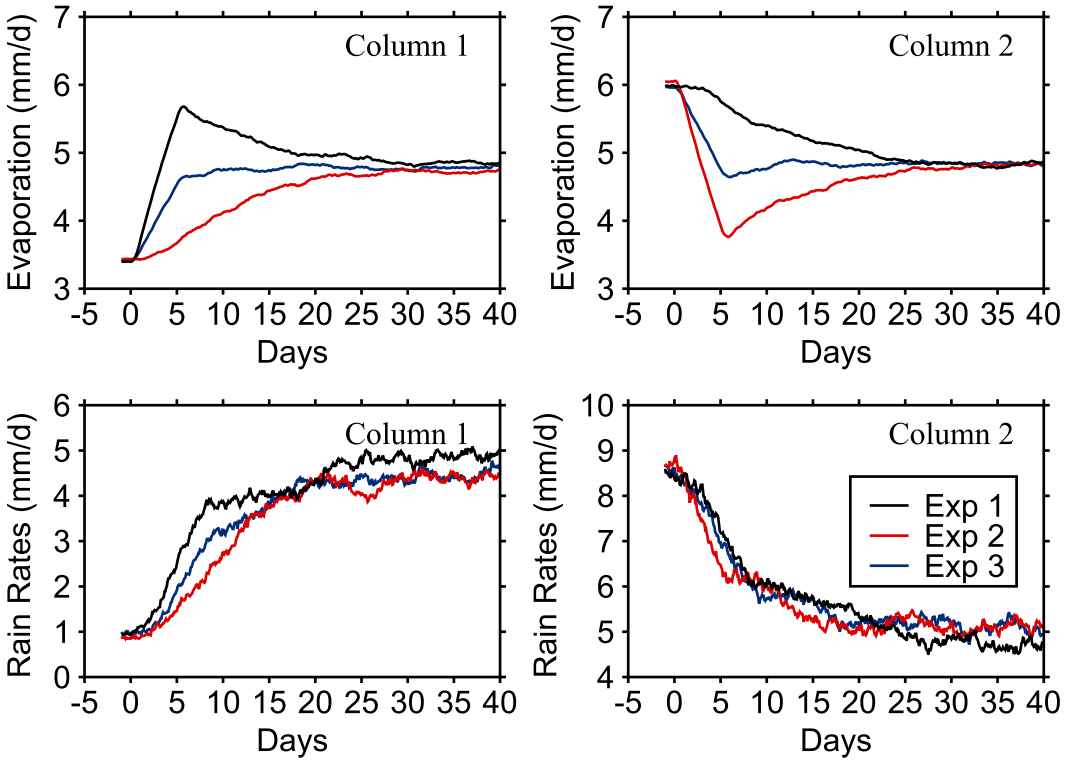

FIG. 11. Time evolution of (top) surface evaporation rates and (bottom) rain rates. The results are the 5-day running mean and ensemble mean for (left) column 1 and (right) column 2 of the experiments 1–3.

where RR_{RCE} is the rain rate at RCE with an SST of 302.7 K and $RR(t < 0)$ is the mean rain rate obtained by averaging over 10 days before the SST is changed. The value of t^* is then estimated as the time when the rain rate is halfway to the RCE value, that is,

$$RR(t^*) = RR^*, \tag{6}$$

with

$$RR^* = RR(t < 0) + \frac{1}{2}RR_d. \tag{7}$$

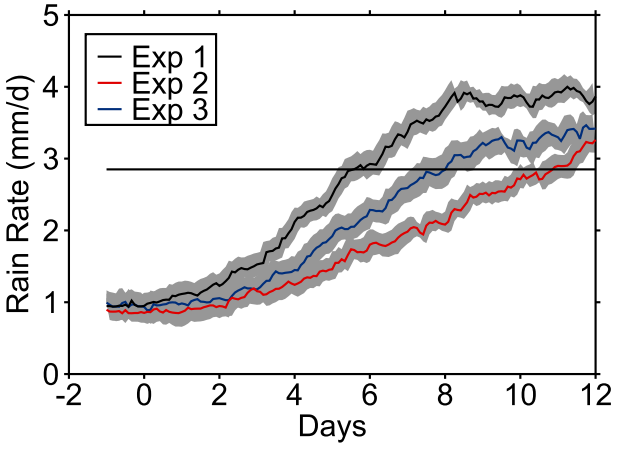

FIG. 12. Time evolution of rain rates. The results are the 5-day running mean and ensemble mean (solid curves) for column 1 of experiments 1–3. The shaded areas represent the range of the five ensemble realizations. The horizontal line represents the value of $RR^* = 2.85\,\text{mm day}^{-1}$.

In this study $RR^* = 2.85\,\text{mm day}^{-1}$.

The values of t^* obtained in experiments 1–3 are listed in Table 3. The range of the five ensemble realizations is also listed. In this study, the transition time varies between 5 and 11 days.

The present idealized experimental setup allows the transition from suppressed to active convection to occur slowly over a time scale characterizing changes in the strength of the large-scale circulation that might develop over a warm pool. However, as presented in section 3, the transition mechanism is more effective when the

TABLE 3. Transition time (days). The values in parentheses represent the range of the five ensemble realizations.

	Experiment		
	1	2	3
Transition time	5.4 (5.0–6.2)	10.9 (10.0–11.6)	8.0 (7.1–8.4)

TABLE 4. Values of SST (K) for columns 1 and 2 before the SST is changed and at the end of simulations that apply the locally and remotely forced transition methods with fixed profiles of heating and moistening rates from the large-scale circulation (experiments 1a and 2a, respectively) and at the end of the simulation that applied the locally forced transition method with a fixed profile of moistening rates from the large-scale circulation (experiment 1b).

	Experiment		
	1a	2a	1b
Methods	Local forcing with fixed large-scale heating and moistening rates	Remote forcing with fixed large-scale heating and moistening rates	Local forcing with fixed large-scale moistening rates
SST_{i_1}	300.7	302.7	300.7
SST_{i_2}	302.7	304.7	302.7
SST_{f_1}	302.7	302.7	302.7
SST_{f_2}	302.7	302.7	302.7

system is forced locally. As a result, the value of t^* in experiment 1 is 5.4 days, almost half the value obtained in the remotely forced experiment. The value of t^* in experiment 3 is halfway between the values obtained in experiments 1 and 2. On the other hand, as presented in section 3a, temperature and humidity perturbations resulting from the large-scale circulation affect the convection and delay the transition to deep convection. As an example, the transition time in an experiment that applies the local forcing and does not apply the heating and moistening rates from the large-scale circulation from day 0 is about 2.5 days shorter than the value obtained in experiment 1 (compare the dashed and solid curves in the bottom-left panel of Fig. 6).

5. The roles of surface forcing and large-scale forcing

In column 1 of experiment 1, the change in convection is a response to the change in underlying SST and to the resulting change in large-scale circulation. However, in column 1 of experiment 2, the change in convection is

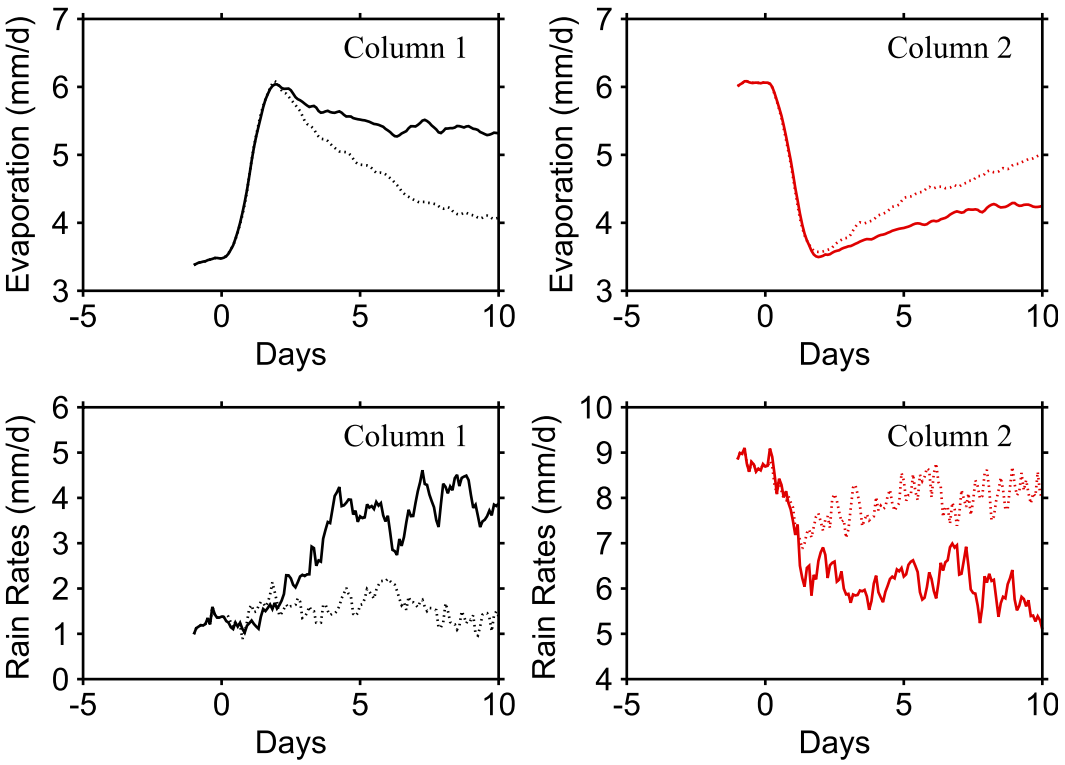

FIG. 13. Time evolution of the daily mean and ensemble mean of (top) surface evaporation and (bottom) rain rates. The results are for (left) the dry column or column 1 of experiments 1 (solid black curves) and 1a (dotted black curves) and (right) the wet column or column 2 of experiments 2 (solid red curves) and 2a (dotted red curves).

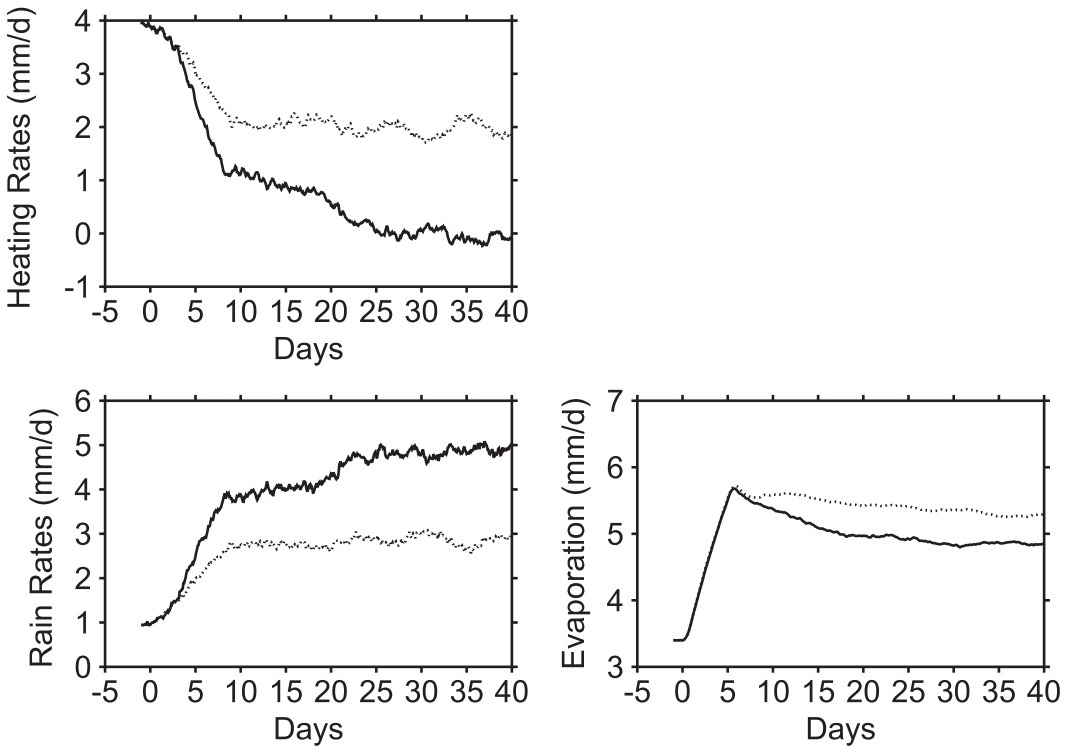

FIG. 14. Time evolution of column-integrated heating rates from the (top) large-scale circulation, (bottom left) rain rates, and (bottom right) surface evaporation. These results are the 5-day running mean and ensemble mean for the dry column of experiments 1 (solid curves) and 1b (dotted curves).

a response to only a change in large-scale circulation. Table 4 presents the list of additional experiments that have been conducted in order to isolate the contributions from the change in SST and the contributions from the evolving large-scale circulation. Experiments 1a and 2a are the repeated versions of experiments 1 and 2, respectively, but from day 0 the profiles of heating and moistening rates from the large-scale circulation are held fixed to those obtained by averaging over 10 days before the SST change is made.

The dotted curves in Fig. 13 illustrate the evolution of surface evaporation (top panels) and rain rates (bottom panels) in the dry column (column 1) of experiment 1a and in the wet column (column 2) of experiment 2a. They are compared to the time evolution of surface evaporation and rain rates in the dry column of experiment 1 (solid curves in left panels) and in the wet column of experiment 2 (solid curves in right panels). The response to the change in SST is effective over the first few days, the period of time over which evaporation rates increase sharply in the dry column of experiment 1a and decrease sharply in the wet column of experiment 2a. Afterward, the effect of the change in SST wanes and, as expected from the heat and moisture budgets, surface evaporation and rain rates in the columns adjust toward the values they had before the SST is changed, but the mean state can be different because of the different underlying SST. The analysis of the time–height cross sections of heating rates from microphysics (results not shown) reveals that the transition process never occurs in experiments 1a and 2a. Hence, the change in the strength of the large-scale circulation is a key component in making the transition in experiments 1–3.

The change in SST drives surface evaporation, which in turn drives changes to the column water vapor. Similarly to the results of Raymond (2000), the adjustment time for moisture in a clear and dry column is much longer than the adjustment time for moisture in a column with preexisting heavy precipitation. Hence, the first phase of the response of convection in the dry column is to recharge moisture in the column rather than increasing the rain rate. As a result, over the first few days, a change in SST produces much larger changes in precipitation in the wet column of experiment 2a than in the dry column of experiment 1a.

Experiments 1a and 2a illustrate the contributions from the change in SST and the influence of the large-scale circulation on the transition mechanism. It may be recalled that in this study the WTG-derived large-scale circulation transports both heat and moisture horizontally

between the columns. A useful further step is therefore to uncouple the contributions from the evolving large-scale heat transport and the contributions from the large-scale moisture transport. Experiment 1b is a repeated version of experiment 1, but from day 0 the profile of moistening rates from the large-scale circulation is held fixed to the profile obtained by averaging over 10 days before the SST is changed, while the large-scale heating rates remain free to evolve according to the WTG calculations. Experiment 1b illustrates the contributions from the large-scale heat transport.

Figure 14 shows the evolution of the heating rates from the large-scale circulation, surface evaporation, and rain rates for the dry column of experiments 1 (solid curves) and 1b (dotted curves). A new quasi-equilibrium state is reached in experiment 1b before day 30, and mean statistics are obtained by averaging over days 30–40. The change in SST causes a reduction of the heating rates from the large-scale circulation. However, its mean value at equilibrium is about 2 mm day^{-1} (a value that is nearly half the value at the initial state) compared to the value of approximately 0 mm day^{-1} obtained at the equilibrium of experiment 1. As a result, convection in the dry column of experiment 1b cannot be driven to the same level of activity as that in the dry column of experiment 1. The mean rain rate at equilibrium is only 2.91 mm day^{-1}, an increase of about 1.9 mm day^{-1} to the mean rain rate at day 0. To balance the fixed drying from the large-scale circulation that is prescribed from day 0 onward, surface evaporation is increased by about 1.9 mm day^{-1}, now 5.25 mm day^{-1}. This value of mean rain rate at equilibrium is almost halfway in between 0.98 and 4.8 mm day^{-1}, which are the values of mean rain rates obtained by averaging over 10 days before the SST is changed and over days 30–40 in the dry column of experiment 1. Hence, the contributions from the large-scale circulation are about equally divided between temperature and moisture effects.

6. Conclusions

This paper presents and discusses the results of idealized 2D CRM simulations of the transition from suppressed to active convection under the influence of the WTG-derived large-scale circulation. The simulations of the transition are initialized from the quasi-steady states of the coupled-column simulations over nonuniform surface forcing. The transition to active convection is forced in the column with suppressed convection by changing surface forcing to a uniform surface forcing across the two columns. The results show that the change in surface forcing drives a subsequent change in the strength of the WTG-derived large-scale circulation. In each simulation of the transition, the strength of the large-scale circulation is reduced to nearly zero. However, this reduction occurs over a period long enough to delay substantially the transition time relative to a simulation performed without applying the heating and moistening rates from the large-scale circulation. During the transition period, early convection recharges moisture into the dry column until the column becomes moist enough to support and sustain deep convection.

As in other studies of the transition from suppressed to active convection, a simulation is performed in which the transition is forced by increasing the local surface forcing, but in addition, this study considers the effects of a large-scale circulation that evolves in response to the change in surface conditions. Such a study provides a more realistic representation of what will happen in the tropical atmosphere. As the local surface forcing is increased to the value in the remote column, surface evaporation overshoots in the dry column and convection becomes more active. However, during the first few days when the large-scale circulation remains in place and produces descent in the dry column, convective cells stop just above the boundary layer top, despite the important amount of CAPE in the sounding. As a result, the first apparent change in the heating rate from microphysics is not observed until around day 2. As the strength of the large-scale forcing is reduced, convection gradually develops with cloud tops above the freezing level at day 3. Later, surface evaporation starts to decrease while rain rate continues to increase toward the mean values obtained in the uncoupled control simulation. In the wet column, surface evaporation and rain rates decrease monotonically toward the values obtained at equilibrium in the uncoupled control simulation.

The evolution of convection in the dry column of the simulation that applied the locally forced transition method is the response to the change in the underlying surface forcing and the resulting changes in the strength of the large-scale circulation. However, this study proposed the coupled-column configuration as a tool to study the influence on local convection of changes in remote convection. We performed an additional simulation in which the transition is forced by decreasing the remote surface forcing. In this simulation, the evolution of convection in the dry column is a response to a change in the strength of the large-scale circulation only. The coupled-column configuration also allows the transition to be forced by increasing the local surface forcing while simultaneously decreasing the remote surface forcing.

The evolution of convection in the dry column of the simulations that applied the locally, remotely, and locally and remotely forced transition methods has been evaluated by defining the transition time, which is the time

when the rain rate is halfway to the value obtained in the uncoupled control run. It is found that the thermodynamic state in the dry column evolves over a period of time, characterizing changes in the strength of the large-scale circulation. The transition time is sensitive to the methods applied to force the transition. For instance, it is around twice as long in the simulation that applied the remotely forced transition method, and simulations that applied the locally and remotely forced transition methods produce intermediate transition times.

The contributions from surface forcing, large-scale heat transport, and large-scale moisture transport have been isolated. The change in surface forcing does not force the transition to deep convection. The response to the change in surface forcing is effective during the first few days only. Afterward, it is the evolution of the large-scale circulation that systematically modulates the transition from suppressed to active convection. Its contributions are approximately equally divided between the heating and the moistening effects of the circulation.

Acknowledgments. We thank the Met Office for the availability of the LEM, version 2.4. C.L.D. was funded by the University of Reading Postgraduate Studentship (International). S.J.W. was funded by the National Centre for Atmospheric Science, a NERC collaborative center.

REFERENCES

Bechtold, P., N. Semane, and S. Malardel, 2013: Convection and waves on small planets and the real earth. *ECMWF Newsletter,* No. 135, ECMWF, Reading, United Kingdom, 14–19.

Bretherton, C., and P. Smolarkiewcz, 1989: Gravity waves, compensating subsidence and detrainment around cumulus clouds. *J. Atmos. Sci.,* **46,** 740–759, doi:10.1175/1520-0469(1989)046<0740:GWCSAD>2.0.CO;2.

Brown, P., and A. Heymsfield, 2001: The microphysical properties of tropical convective anvil cirrus: A comparison of models and observations. *Quart. J. Roy. Meteor. Soc.,* **127,** 1535–1550, doi:10.1002/qj.49712757504.

Daleu, C., 2013: Simulations of interacting regions of tropical deep convection coupled by a weak-temperature gradient parameterization of the large-scale circulation. Ph.D. thesis, University of Reading, 50 pp.

——, S. Woolnough, and R. Plant, 2012: Cloud-resolving model simulations with one and two-way couplings via the weak temperature gradient approximation. *J. Atmos. Sci.,* **69,** 3683–3699, doi:10.1175/JAS-D-12-058.1.

Fridlind, A., and Coauthors, 2012: A comparison of TWP-ICE observational data with cloud-resolving model results. *J. Geophys. Res.,* **117,** D05204, doi:10.1029/2011JD016595.

Grabowski, W., X. Wu, M. Moncrieff, and W. Hall, 1998: Cloud-resolving modeling of cloud systems during phase III of GATE. Part II: Effects of resolution and the third spatial dimension. *J. Atmos. Sci.,* **55,** 3264–3282, doi:10.1175/1520-0469(1998)055<3264:CRMOCS>2.0.CO;2.

——, and Coauthors, 2006: Daytime convective development over land: A model intercomparison based on LBA observations. *Quart. J. Roy. Meteor. Soc.,* **132,** 317–344, doi:10.1256/qj.04.147.

Gray, M., J. Petch, S. H. Derbyshire, A. R. Brown, A. P. Lock, H. A. Swann, and P. R. A. Brown, 2001: Version 2.3 of the Met Office Large Eddy Model: Part II: Scientific documentation. APR Turbulence and Diffusion Note 276, Met Office, Reading, United Kingdom, 48 pp.

Gregory, D., and P. R. Rowntree, 1990: A mass flux convection scheme with representation of cloud ensemble characteristics and stability-dependent closure. *Mon. Wea. Rev.,* **118,** 1483–1506, doi:10.1175/1520-0493(1990)118<1483:AMFCSW>2.0.CO;2.

Holloway, C., S. Woolnough, and G. Lister, 2012: Precipitation distributions for explicit versus parametrized convection in a large-domain high-resolution tropical case study. *Quart. J. Roy. Meteor. Soc.,* **138,** 1692–1708, doi:10.1002/qj.1903.

Kain, J. S., 2004: The Kain–Fritsch convective parameterization: An update. *J. Appl. Meteor.,* **43,** 170–181, doi:10.1175/1520-0450(2004)043<0170:TKCPAU>2.0.CO;2.

Khairoutdinov, M., and D. Randall, 2006: High-resolution simulation of shallow-to-deep convection transition over land. *J. Atmos. Sci.,* **63,** 3421–3436, doi:10.1175/JAS3810.1.

Kuang, Z., 2012: Weakly forced mock walker cells. *J. Atmos. Sci.,* **69,** 2759–2786, doi:10.1175/JAS-D-11-0307.1.

——, and C. Bretherton, 2006: A mass-flux scheme view of a high-resolution simulation of a transition from shallow to deep cumulus convection. *J. Atmos. Sci.,* **63,** 1895–1909, doi:10.1175/JAS3723.1.

——, P. Blossey, and C. Bretherton, 2005: A new approach for 3D cloud-resolving simulations of large-scale atmospheric circulation. *Geophys. Res. Lett.,* **32,** L02809, doi:10.1029/2004GL021024.

Liu, P., and Coauthors, 2009: An MJO simulated by the NICAM at 14- and 7-km resolutions. *Mon. Wea. Rev.,* **137,** 3254–3268, doi:10.1175/2009MWR2965.1.

Mapes, B., and R. Houze Jr., 1995: Diabatic divergence profiles in western Pacific mesoscale convective systems. *J. Atmos. Sci.,* **52,** 1807–1828, doi:10.1175/1520-0469(1995)052<1807:DDPIWP>2.0.CO;2.

——, and X. Wu, 2001: Convective eddy momentum tendencies in long cloud-resolving model simulations. *J. Atmos. Sci.,* **58,** 517–526, doi:10.1175/1520-0469(2001)058<0517:NACCEM>2.0.CO;2.

Petch, J., and M. Gray, 2001: Sensitivity studies using a cloud-resolving model simulation of the tropical west pacific. *Quart. J. Roy. Meteor. Soc.,* **127,** 2287–2306, doi:10.1002/qj.49712757705.

Ramsay, H., and A. Sobel, 2011: Effects of relative and absolute sea surface temperature on tropical cyclone potential intensity using a single-column model. *J. Climate,* **24,** 183–193, doi:10.1175/2010JCLI3690.1.

Randall, D., M. Khairoutdinov, A. Arakawa, and W. Grabowski, 2003: Breaking the cloud parameterization deadlock. *Bull. Amer. Meteor. Soc.,* **84,** 1547–1564, doi:10.1175/BAMS-84-11-1547.

Raymond, D., 2000: Thermodynamic control of tropical rainfall. *Quart. J. Roy. Meteor. Soc.,* **126,** 889–898, doi:10.1002/qj.49712656406.

——, and X. Zeng, 2005: Modelling tropical atmospheric convection in the context of the weak temperature gradient approximation. *Quart. J. Roy. Meteor. Soc.,* **131,** 1301–1320, doi:10.1256/qj.03.97.

Redelsperger, J.-L., and Coauthors, 2000: A GCSS model intercomparison for a tropical squall line observed during

TOGA-COARE. I: Cloud-Resolving Models. *Quart. J. Roy. Meteor. Soc.,* **126,** 823–863, doi:10.1002/qj.49712656404.

Robe, F., and K. Emanuel, 2001: The effect of vertical wind shear on radiative–convective equilibrium states. *J. Atmos. Sci.,* **58,** 1427–1445, doi:10.1175/1520-0469(2001)058<1427:TEOVWS>2.0.CO;2.

Rotunno, R., J. Klemp, and M. Weisman, 1988: A theory for strong, long-lived squall lines. *J. Atmos. Sci.,* **45,** 463–485, doi:10.1175/1520-0469(1988)045<0463:ATFSLL>2.0.CO;2.

Sessions, S., S. Sugaya, D. Raymond, and A. Sobel, 2010: Multiple equilibria in a cloud-resolving model using the weak temperature gradient approximation. *J. Geophys. Res.,* **115,** D12110, doi:10.1029/2009JD013376.

Shutts, G., and M. Gray, 1994: A numerical modelling study of the geostrophic adjustment process following deep convection. *Quart. J. Roy. Meteor. Soc.,* **120,** 1145–1178.

Sobel, A., and C. Bretherton, 2000: Modeling tropical precipitation in a single column. *J. Climate,* **13,** 4378–4392, doi:10.1175/1520-0442(2000)013<4378:MTPIAS>2.0.CO;2.

——, G. Bellon, and J. Bacmeister, 2007: Multiple equilibria in a single-column model of the tropical atmosphere. *Geophys. Res. Lett.,* **34,** L22804, doi:10.1029/2007GL031320.

Swann, H., 1998: Sensitivity to the representation of precipitating ice in CRM simulations of deep convection. *Atmos. Res.,* **47–48,** 415–435, doi:10.1016/S0169-8095(98)00050-7.

Tao, W., J. Simpson, C. Sui, C. Shie, B. Zhou, K. Lau, and M. Moncrieff, 1999: Equilibrium states simulated by cloud-resolving models. *J. Atmos. Sci.,* **56,** 3128–3139, doi:10.1175/1520-0469(1999)056<3128:ESSBCR>2.0.CO;2.

Tiedtke, M., 1989: A comprehensive mass flux scheme for cumulus parameterization in large-scale models. *Mon. Wea. Rev.,* **117,** 1779–1800, doi:10.1175/1520-0493(1989)117<1779:ACMFSF>2.0.CO;2.

Tompkins, A., 2000: The impact of dimensionality on long-term cloud-resolving model simulations. *Mon. Wea. Rev.,* **128,** 1521–1535, doi:10.1175/1520-0493(2000)128<1521:TIODOL>2.0.CO;2.

Wang, S., and A. H. Sobel, 2011: Response of convection to relative sea surface temperature: Cloud-resolving simulations in two and three dimensions. *J. Geophys. Res.,* **116,** D11119, doi:10.1029/2010JD015347.

——, ——, and Z. Kuang, 2013: Cloud-resolving simulation of TOGA-COARE using parameterized large-scale dynamics. *J. Geophys. Res. Atmos.,* **118,** 6290–6301, doi:10.1002/jgrd.50510.

Woolnough, S., and Coauthors, 2010: Modelling convective processes during the suppressed phase of a Madden–Julian oscillation: Comparing single-column models with cloud-resolving models. *Quart. J. Roy. Meteor. Soc.,* **136,** 333–353, doi:10.1002/qj.568.

Wu, C., B. Stevens, and A. Arakawa, 2009: What controls the transition from shallow to deep convection? *J. Atmos. Sci.,* **66,** 1793–1806, doi:10.1175/2008JAS2945.1.

Yano, J.-I., and M. Bonazzola, 2009: Scale analysis for the large-scale tropical atmospheric dynamics. *J. Atmos. Sci.,* **66,** 159–172, doi:10.1175/2008JAS2687.1.